



UNIVERSITY OF
BIRMINGHAM

Characterizing the single cell transcriptional landscape of NK cells in chemotherapy-exposed/naïve tumor microenvironments

a pan cancer assessment

By

Chisanu Thumarat

ID: 2588815

Supervised by

Dr. Wayne Croft and Dr. Jianmin Zuo

Dissertation submitted for the requirements of the degree of
Master of Science in Bioinformatics

University of Birmingham

August 2024

Table of Contents

	Page
• Abstract	2
• Introduction	3
• Objective	7
• Methodology	8
• Results	15
• Discussion	39
• Conclusion	42
• Acknowledgement	43
• Code availability	43
• Supplementary data availability	43
• Appendix	44
○ Supplementary figures	
• References	47

Abstract

Natural killer (NK) cells are instrumental in tumor eradication by the immune system, characterized by their innate ability to kill cancer cells without prior sensitization. However, within various tumor microenvironments (TMEs), NK cell functions often become impaired due to immune modulation and suppression, which promote tumor growth. This study examines the restoration of NK cell functionality by neoadjuvant chemotherapy (NACT), highlighting its potential as a therapeutic target. Employing single-cell transcriptomic profiles from 25 samples across five tissue types from three primary sites—esophagus, pancreas, and omentum—we identified nine distinct NK functional states. Chemotherapy was observed to enhance NK cytotoxicity and activation, albeit with adverse effects on cellular viability. Through pathway analysis, differential expression analysis, and AUCells gene set scoring, we characterized a subpopulation of NK cells, defined as CD56⁻, CD16^{bright} with the stress activator molecule DNAJB1⁺, known as tumor-associated NK (TaNK) cells, which exhibit novel dynamic behaviors. Despite these insights into functional variability, no significant alterations in NK cell proportions were detected. This study underscores the utility of single-cell transcriptomics in advancing our understanding of NK cell dynamics within TMEs and suggests how both TMEs and chemotherapy can be harnessed to identify potential targets for immunotherapy.

Introduction

Natural killer cells (NK) are a vital component of the innate immune response against tumor progression. Through MHC-independent interaction, functional NK cells are capable of unrestricted cancer cell killing and represent a promising therapeutic strategy¹. NK cell-mediated immune responses involve 3 major NK-cell-intrinsic competencies. Firstly, through “missing-self recognition”, it is a process of losing inhibitory signaling from certain cells without MHC-I expression under stress conditions^{2, 3}. Secondly, is to distinguish self- or pathogen-expressed biomolecules. Under normal conditions, NK cells exhibit “self-tolerance” through inhibitory receptors such as killer cell immunoglobulin-like receptors (KIRs) and C-type lectin receptors (e.g., CD94, NKG2A), which recognize self-MHC molecules^{4, 5}. Additionally, immunomodulatory molecules like CD47, known as a 'don't eat me' signal on red blood cells and other hematopoietic cells⁶, further prevent unnecessary immune attacks, ensuring that NK cells do not target healthy self-cells. In pathogenic condition, however, pathogen-related biomolecules from infected or stressed/transformed cells will be upregulated and secreted. This leads to the third crucial capability: “stress-induced activation”, where NK cells respond to upregulated stress ligands on infected or transformed cells, initiating NK cell-mediated cytotoxicity⁷. These three abilities — missing-self recognition, self-tolerance, and stress-induced activation — work together in harmony to ensure a precise and robust immune response. This finely tuned interplay allows NK cells to differentiate between healthy cells, infected cells, or transformed cells effectively⁸.

However, in the tumor microenvironment (TME) of several cancers, these NK cell abilities are notably compromised, which complicates tumor clearance and medical intervention. The TME plays a crucial role in determining the affected patient's immune-mediated response against tumors⁹. It is characterized by a variety of mechanisms that suppress

NK cell functionality, including immune suppression, immuno-editing, immune exhaustion, and the rapid evolution of tumors to become poorly immunogenic—a process known as immune subversion¹⁰. Moreover, tumors tend to suppress immune cells in a manner consistent with the discontinuity theory of immunity, where immune responses are initially strong in sudden onset but wane in prolonged activation^{11, 12}. These dynamics pose additional challenges for sustaining effective NK cell responses over the course of cancer progression (Fig. 1).

Neoadjuvant chemotherapy (NACT) plays a nuanced role in cancer treatment. While its primary objective is to reduce tumor size, it also significantly impacts the tumor microenvironment and immune dynamics¹³. Essentially, chemotherapy can facilitate tumor inflammation, which, although it may initially suppress immune cell functions, also helps restore immune responses, as evidenced by several studies^{14, 15}. This inflammation is pivotal for inducing immunologic cell death, creating conditions that restore the three principal NK cell functions—missing-self recognition, self-tolerance, and stress-induced activation¹⁶. These effects are critical as they help counteract the suppression of NK cell activity commonly observed in the tumor microenvironment, thereby enhancing both the direct cytotoxic impact on tumor cells and the broader immune surveillance capabilities of NK cells^{17, 18}. By reducing tumor burden and altering stromal conditions, neoadjuvant chemotherapy enhances tumor targeting and bolsters the immune system's capacity to combat cancer. Nonetheless, cancer patients frequently experience relapse during the course of their disease¹⁹, underscoring the critical need for alternative therapeutic strategies²⁰.

Recent investigations, particularly those utilizing single-cell analyses, have revealed significant heterogeneity in NK cell behavior across different tumors^{21, 22}. This variability underscores the need for precision in immunotherapy approaches. For example, immature CD56^{bright}CD16^{lo} NK cells were largely predominant in nasopharyngeal cancer and basal cell carcinoma, whereas the mature CD56^{dim}CD16^{hi} NK cells occupied renal carcinoma and lung

cancer²³. These findings, consistent with previous studies^{24, 25}, highlight the potential for tailored therapeutic strategies that not only address the generic properties of tumor microenvironment but also consider the specific immune context of each cancer type. Such distinctions are crucial for developing more effective and individualized treatments, optimizing NK cell-based therapies to exploit their full therapeutic potential.

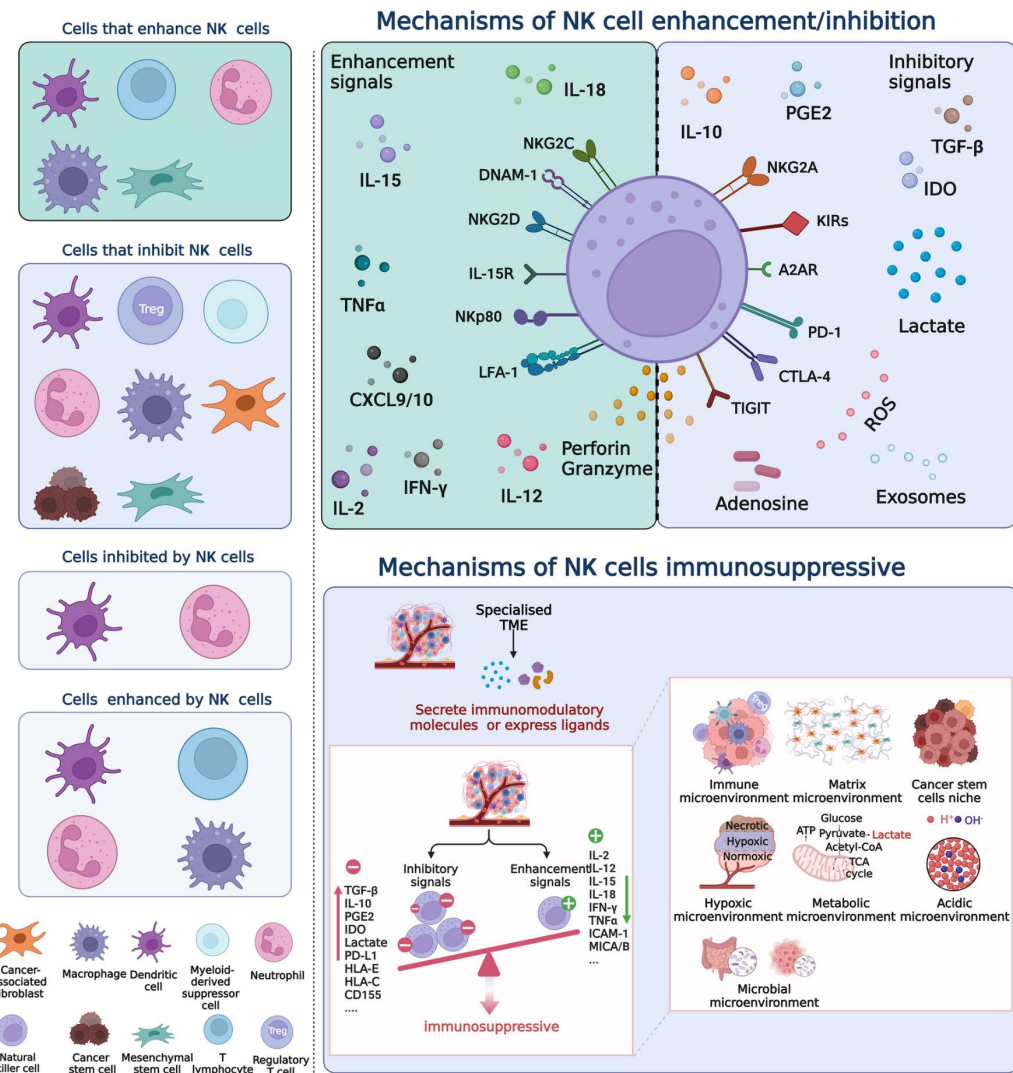


Figure 1: NK cell functional dynamics within tumor microenvironment (TME)¹⁰

Objectives

We aim to profile the transcriptional state of NK cells at the single-cell level with the following objectives:

1. To determine whether transcriptional profiles of NK cells differ across various tumor types.
2. To identify consistent signatures of NK cell dysfunction and propose potential signaling targets for therapeutic intervention.
3. To detect tumor-specific or pan-tumor-type changes in NK cell function driven by chemotherapy based on single cell transcriptomics.

To achieve these objectives, we have generated single-cell transcriptomics data from 4 distinct tumor microenvironments from various tumor sites: High-Grade Serous Ovarian Cancer (HGSOC), Esophageal Adenocarcinoma (EAC), Benign pancreatic tumor (Benign), Pancreatic Ductal Adenocarcinoma (PDAC), and gastrointestinal metastatic to omentum (GI_MET). Additionally, adjacent normal (Norm) from esophageal and omentum tissue will be included in this study, allowing for a comprehensive comparison across different statuses. This comprehensive dataset will help bridge knowledge gaps and create an atlas for NK cell-based immunotherapy, potentially translating these findings into clinical practice.

Methodology

Data type

Sample processing was carried out by Genomics Birmingham (University of Birmingham, UK). Single-cell transcriptome profiling was completed using a Chromium Controller and Chromium Single Cell 3' Library & Gel Bead Kit v2 (10x Genomics) and sequenced on an Illumina NextSeq 500 with a sequencing depth of 20,000 raw reads per cell. Raw data were processed with Cell Ranger v7.1.1, aligning to the GRCh38 reference genome to produce unique molecular identifier (UMI) count matrices for each sample.

Samples based on primary tissue source and chemotherapy treated (CT) / treatment-naïve (TN) status consisted of:

1. Omentum (n=10): High Grade Serous Ovarian Cancer (HGSOC, n=4 (CT), 4 (TN)), Gastrointestinal metastasis (GI_MET, n=1 (TN)), Normal (Norm, n=1(CT))
2. Esophagus (n=10): Esophageal Adenocarcinoma (EAC, n=4 (CT), n=4 (TN)), Adjacent Normal (Norm, n=1 (CT), n=1 (TN))
3. Pancreas (n=5): Pancreatic Ductal Adenocarcinoma (PDAC, n=4 (TN)), Benign (Benign, n=1 (TN))

scRNA-seq data pre-processing

Data pre-processing and analysis were conducted using R (v4.1.1)²⁶. The pre-processing steps, dimensional reduction, unsupervised clustering, differential expression analysis, and data visualization were all performed using Seurat (v5.0.3)²⁷, unless otherwise specified. Quality control measures included excluding outlier cells with unique RNA feature counts outside the range of 300 to 3,500, and with mitochondrial RNA content below 10%. DoubletFinder

(v2.0.4)²⁸ was used for detecting and excluding doublets, ensuring the dataset consisted only of singlets. Data were normalized, and high variable genes (HVGs) were identified using SCTtransform (v0.4.1)^{29, 30} with mitochondrial gene regression, using default parameters.

Integration and unsupervised clustering

Data integration was achieved using Harmony (v0.1.1)³¹, which aligns datasets from different sources or conditions by correcting for batch effects. Principal component analysis (PCA) was then performed, capturing the first 50 principal components to retain comprehensive variability for downstream analyses. For unsupervised clustering, the SCT assay was employed within Seurat. Dimensional reduction and visualization of the clusters were conducted using Uniform Manifold Approximation and Projection (UMAP), embeddings into Harmony reduction. Cell clusters were systematically identified through Seurat's FindNeighbors and FindClusters functions, with a resolution parameter set at 0.5.

Major lineage cell type clusters were identified using a panel of canonical marker genes^{32, 33} for each lineage: T cells (*CD3D*), B cells (*MS4AI*), plasma- blasts (*IGKC*), epithelial cells (*EPCAM*), proliferating cells (*MKI67*), endothelial cells (*PECAMI*, *COL1A1*), fibroblasts (*DCN*, *COL1A1*, *PDPN*), myeloid cells (*LYZ*), mast cells (*TPSABI*), and immune cells (*PTPRC*). For the identification and isolation of NK and NKT cells, cells were primarily defined by the expression of NK-cell lineage gene set (*GNLY*, *XCL1*, *FGFBP2*).

Given the inherent challenges in distinguishing T-cells from NK and NKT cells due to overlapping marker expressions, iterative refinement in the isolation of NK and NKT cell clusters was necessary. This involved negative selection against T-cell lineage markers *CD3D*, *CD3G* and *CD3E* alongside positive selection for NK functional markers *CD56* (*NCAMI*), *KLRF1*, *KLRK1*, *NKG7*, and *CD16* (*FCGR3A*) (Fig. S1)^{34, 35}. Additionally, a dual-scoring

system was implemented, where cells were evaluated based on low activity of the T-cell lineage gene set or high activity of the NK-cell lineage gene set. This ensured the accurate classification and inclusion of cells exhibiting robust NK cell phenotypes, irrespective of their T-cell marker status. These processes were repeated through four rounds of unsupervised clustering.

Sub-clustering of NK cells, Functional cell signature and Signature gene set definition

Although NK and NKT cells are distinct clusters, NKT cells have shared properties with NK cells^{35, 36}. Therefore, its functional states are considered together as NK molecular profiles in downstream analyses.

In the sub-clustering analysis of NK functional states, clusters were initially visualized and refined using UMAP to aid in identifying distinct functional profiles. These clusters were then defined based on functional signatures derived from 1-vs-all differential expression analyses and verified by previous literature^{23, 37, 38}. Each NK subcluster was characterized by distinct gene sets that represent specific functional aspects of NK cell biology. The gene sets used for NK functional screening include:

1. Cytotoxicity: Key genes include *GNLY*, *GZMA*, *GIMAP7*, *PSMB10*, *TBC1D10C*, *FGFBP2*, *ACTB*, and *CSK*, which are associated with the cytolytic activity of NK cells.
2. Activation: This set includes *CD69*, *NCR1*, *KLRK1*, *CD226*, and *CD96*, along with transcription factors and signaling molecules *FOS*, *IFNG*, *ATF3*, and *IGF1R*, indicating activation states.
3. Chemokines and Receptors: Composed of chemokine genes *XCL1*, *XCL2*, *CCL3*, *CCL4*, *CCL4L2*, and *CCL3L1*, which facilitate the chemotactic response of NK cells.

4. Stress and Exhaustion: Includes stress response and exhaustion markers *HSPA1A*, *HSP90AA1*, *DNAJB1*, and *HSPA1B*, which are crucial for understanding the stress resilience and exhaustion status of NK cells.
5. General NK Cell Markers: A broad set of phenotypic markers *including CD7, NCAM1* (CD56), and *KLRF1*, which are essential for general NK cell phenotyping.
6. Miscellaneous other functional roles: Molecular signaling and regulatory markers include *CRTAM*, *LINC02446*, *RILPL2*, *MAML3*, *B3GNT7*, *SSBP2*, *ABTB2*, *FTH1*, *Clorf21*, *TGFBR3*, *KLF3*, *PEX14*, *OASL*, *WDR47*, and *VPS13D*.

Differential expression analysis

RNA assay has been employed for differential expression analysis. The data will be normalized using a log-transformation with a scaling factor of 10,000. The Variance Stabilizing Transformation method will be applied to rank the top 2,000 high variable genes (HVGs) from the RNA assay. Differential expression analysis was carried out using the Wilcoxon rank sum test (Mann–Whitney U test), a non-parametric test ideally suited for non-normally distributed data, as implemented in the presto R package (v1.0.0)³⁹. Criteria for detecting significant differences included a minimum of 25% average log-scale fold change and detectability in at least 25% of cells within either comparison group. A 5% significance level for a two-tailed test was used, with Bonferroni correction applied to control for multiple testing using all genes in the dataset.

Gene set signature activity scoring

All activity scorings in this study were conducted using AUCell (v1.25.2)⁴⁰ to calculate ranked-based gene set activity scoring. As AUCell operates independently of gene expression units and normalization methods, ranked expression matrices were constructed using RNA assay. Area Under the Curve (AUC) values will be calculated for the top 5% of ranked genes to determine whether the provided signature gene sets are enriched by HVGs in each cell.

Pathway enrichment analysis

Pathway enrichment analysis was conducted using AUCells activity scoring, specifically tailored for single-cell data. This methodological was adaptated from Python's AnnData, developed by Omicverse⁴¹, within this study as R framework.

Pathways were sourced from the molecular signaling database (MsigDB)⁴² utilizing the MSigDBr package (v7.5.1). Analysis was categorized into two groups:

- 1) All Pathway Enrichment: Utilizing curated gene sets (C2) with canonical pathways (CP) and Reactome subset of CP based on ranked gene list of highly variable genes (HVGs) stored in scale.data layer.
- 2) Regulon enrichment analysis: Employing regulatory gene sets (C3), focusing on regulatory elements with transcription factor target (TFT).

Pathway activity ranking and scoring were calculated by AUCells, with matrix storing AUC values for all cells incorporated into the Seurat object as an AUC assay.

The pathway enrichment analysis employed a statistical approach analogous to that used for differential expression of AUC values to handle right-skewed distribution of AUC values, with modified criteria: a minimum of 2% average log-scale fold change, detectability

in at least 25% of cells within either comparison group, a 1% significance level for a two-tailed test, and focusing only on positive differences (only.pos = TRUE). Additionally, a pathway was considered active in a cluster if it showed a mean AUC value exceeding 0.1, with proportion of active cells serving as a secondary criterion to further validate pathway activity.

Top pathway selections for all enrichment activities required:

- 1) Pathway Enrichment: Pathways must exhibit more than 0.2 mean AUC values for at least one cluster, and less than 0.3 mean AUC values across all clusters.
- 2) Regulon Enrichment: Pathways must demonstrate more than 0.1 mean AUC values for at least one cluster, and less than 0.2 mean AUC values across all clusters.

These criteria highlight cluster-specific pathways without uniform presence across clusters, and distinct for each cluster.

The analyses aim to characterize NK molecular heterogeneity based on NK functional cluster influenced by the tumor microenvironment (TME) and chemotherapy effects, ordered into these resolution levels:

- A. NK functional clusters level
 - a. Chemotherapy status level
 - b. Tissue microenvironment level
 - i. Chemotherapy status within each tissue microenvironment level

Only samples from HGSOC, EAC and Norm have been included into the analyses of both TMEs and chemotherapy status, due to be the only TMEs that have both chemotherapy status. Visualization of pathway enrichment analyses was conducted using ggplot2 (v3.5.1)⁴³ and tidyHeatmap (v1.8.1)⁴⁴. Dot plots from ggplot2 displayed mean AUC values and the proportion of cells active for each pathway, while heatmap illustrated relative z-score of mean AUC values.

Proportional analysis

Proportional analysis of cell clusters was conducted to quantify the relative abundance of immune cells, identified by CD45 (*PTPRC*) positive expression, and total NK cells, identified by the results from the fourth round of unsupervised clustering. This analysis assessed the proportions of the immune cell population and NK cell functional states, respectively. Statistical comparisons were performed using the Wilcoxon rank sum test (Mann–Whitney U test), as implemented in the rstatix R package (v0.7.2)⁴⁵. To account for multiple comparisons and control the false discovery rate, a 5% significance level for a two-tailed test and Benjamini-Hochberg correction were applied. Visualization of the proportional analysis results was conducted using ggplot2 (v3.5.1)⁴³.

Statistical Corrections

The choice of statistical correction methods was tailored to the specific needs of each analysis. Bonferroni correction, known for its stringent control of Type I errors, was used in differential expression analysis to minimize the likelihood of false positives in a scenario with a high number of comparisons. Conversely, the Benjamini-Hochberg correction was employed in proportional analysis to effectively control the false discovery rate, providing a balance between discovery and reliability when assessing proportion differences across multiple groups.

Results

Single cell analysis reveals consistent NK cell composition across multiple tumor microenvironments

Unsupervised clustering of single-cell RNA sequencing (scRNA-Seq) data from 172,735 cells by 25 samples, identifies 11 distinct major lineage cell types (Fig. 2A, B). Major lineages were defined by clearly distinguishable lineage markers (Fig. 2C). Additionally, crucial functional NK markers and CD3 family genes further refined the identification of NK and NKT cell clusters (Fig. 2D). Despite challenges in separating NK and NKT clusters from potential T-cell contamination, *CD3D* and T-cell lineage gene sets remain detectably active within these clusters, as shown by their expression and AUC values (Fig. 2E). The high expression of *FCGR3A*, coupled with the active NK-cell lineage gene set, confirms the inclusion of NK and NKT cells within these designated clusters (Fig. 2F). Total 29,367 NK and NKT cell, and their clusters are isolated for subsequent purification and functional NK-focused downstream analyses (Fig. S1).

Cell type composition across different samples revealed variability in the compositions of 146,466 cells in major immune clusters (Fig. 2G). Proportional analyses, stratified by chemotherapy status, and tumor microenvironment, demonstrated no statistically significant differences (Fig. 2H, I). The lack of alteration in the proportional distribution of immune clusters suggests that the impact of these factors is not recognizable in terms of corrected statistics at the gross immune cluster level based on cell type proportions (Table. S1).

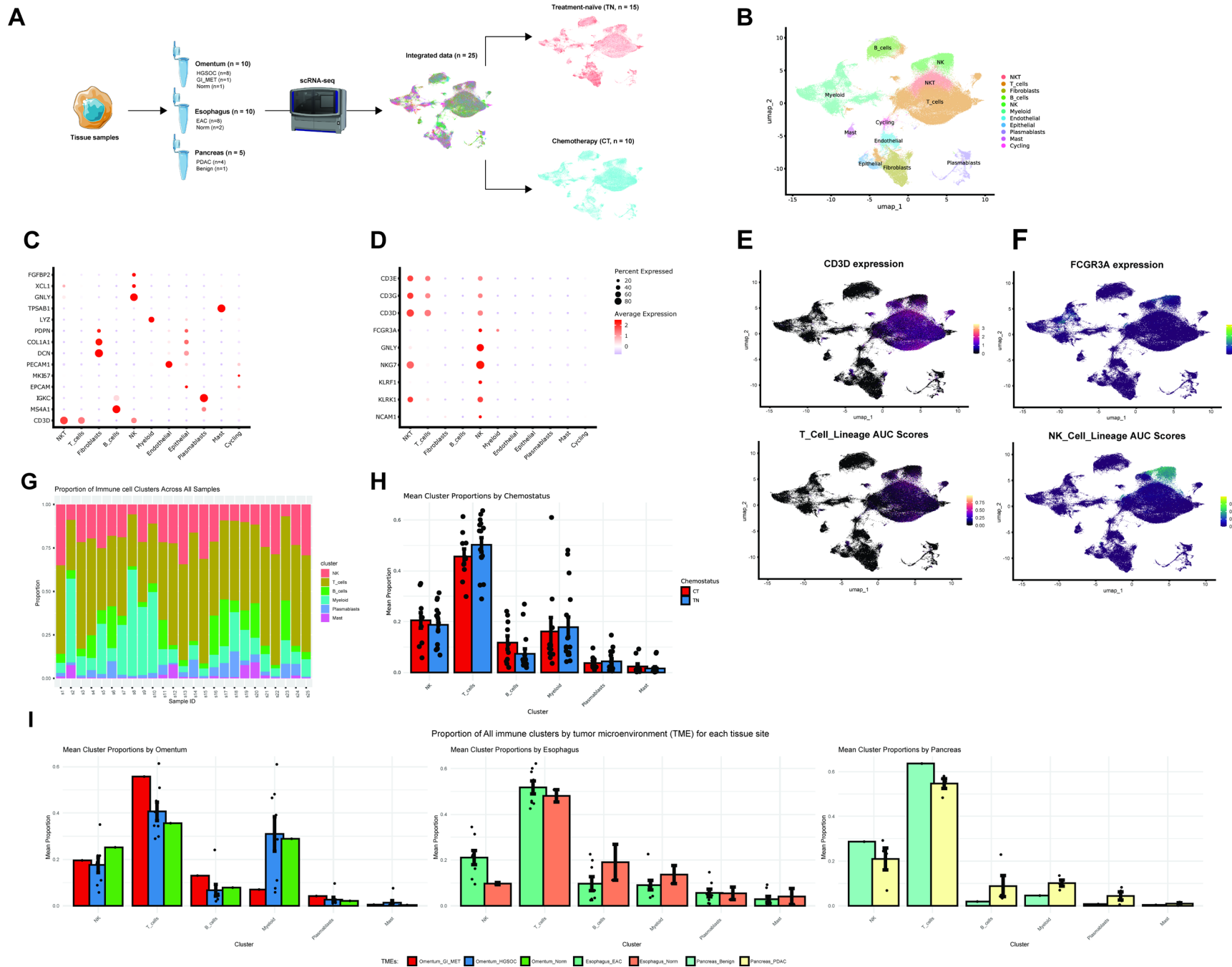


Figure 2: Major Lineage Identification Through Unsupervised Clustering. **A**, Workflow of the study from tissue sample dissociation to single-cell sequencing, categorizing samples based on chemotherapy treatment (CT) and treatment-naïve (TN) status. **B**, UMAP visualization of major lineage cell types, capturing the overall cellular composition. **C**, Mean expression profiles of lineage marker genes alongside the proportion of each cell population. **D**, Mean expression profiles of CD3 gene family and functional NK marker genes, with corresponding population proportions. **E (Top)**, UMAP feature plot showing expression of *CD3D*. **E (Bottom)**, UMAP feature plot illustrating T-cell lineage signature gene set AUC scores. **F (Top)**, UMAP feature plot depicting expression of CD16 (*FCGR3A*). **F (Bottom)**, UMAP feature plot showing NK-cell lineage signature gene set AUC scores. **G**, Proportions of gross immune cells across all samples, Major lineage immune cell type proportion of stratified by chemotherapy status (**H**), and tissue microenvironment (**I**).

Characterization of distinct NK subclusters manifested alterations of NK transcriptomics and functional profiles

Unsupervised clustering on 6,349 final isolated NK and NKT cells identified 9 functional NK populations (Fig. 3). Nine NK transcriptional states were identified (Fig. 3A, B), including Cytotoxic (NKcyt), Exhausted (NKexh), Immature-cytokine-producing (NKimm), Effector-1 (NKeff1), Effector-2 (NKeff2), Memory (NKmem), Residence (NKres), and Activated-immature (NKact). Distinct transcriptional profile of the NK cell clusters was evident from the top 10 differentially expressed genes (DEGs) for each cluster (Fig. 3C), and clusters were further characterized by eight functional gene sets stated previously, were utilized instead of representative functional NK markers (Fig. 3D). The results captured functional state in agreement with both previous studies²³, and DEGs listed for all NK states in Figure 3A. Notably, cytotoxic NK cells, are defined by having very high cytotoxicity gene set expression (*GNLY*^{high}, *GZMA*^{high} and *ACTB*^{high}, in particular) and double CD16 (*FCGR3A*) and CD56 (*NCAMI*) positive⁴⁶. Previously reported 3 NK functional subpopulations are pulled out. One of the most important NK cells in this tumor immunology field, tumor-associated NK cells (TaNK)⁴⁷ are identified in this study as NK effector-2 cells. This is due to an extension from previously reported by using CD56⁻, CD16^{bright} with stress activator molecule *DNAJB1* for TaNK identification by pan-cancer NK analysis publication²³, altogether with having activating receptors: *NCR1*^{high}, DNAM-1^{high} (*CD226*) and *CD69*^{high} expression. Additionally, this TaNK-like effector-2 cells seems to be close to NK effector-1 cells, characterized similar to effector-2, but without *DNAJB1* and *GZMA* positive expression. In contrast, *KLRC2* and *PDCD1* are claimed to be not expressed in this cluster, suggesting a dynamic profiling of TaNK identities.

Gene set scoring was confirmed to support functional characterization of TaNK (Fig. 3E). Cytotoxicity is which mainly active within cytotoxic NK cell cluster are partly presented

in NK effector-2 as well, due to terminal TaNK documented to becoming less to non-cytotoxic in terminal phenotype, but more stressed, with some activated capabilities, supporting possibilities of dynamics functional profile within effector-2 cluster. Second cluster is immature NK cells, defined by having CD56^{bright} and CD16⁻, a characteristic of not fully mature NK cells. This NK cluster also reported in pan-cancer NK study, and other studies as immature blood infiltrated NK cells with cytokine producing capabilities⁴⁸. Lastly, exhausted NK cells are characterized by overwhelmingly high stress response gene set expression, and CD56⁻ with CD16^{low} expression, this cluster is also another prominent cluster, especially in tumor research⁴⁹. The gene set profiling of this stressed NK cluster supports an ongoing suppression of 3 principal NK cell functionalities, with prominent stress gene sets, while suppressing almost all genes expression from other NK functionality gene sets. Clusters that could not be accurately assigned a functional state grouping were considered intermediates between state and annotated as “Unknown”.

Proportions of NK clusters among different samples revealed diversity in the composition of NK functional clusters (Fig. 3F). Proportional analyses showed no statistically significant differences across chemotherapy status and tissue microenvironment (Fig. 3G, H, Table. S1). Not only lack of alteration in the proportional distribution will suggests barely noticeable alteration statically, but the present of a warrant mentioned cluster, NKexh at slightly lower proportional tendencies in normal tissue microenvironment compared to the other TMEs within the same tissue site, suggested the possible alternative molecular alteration in Omentum tissue than other places.

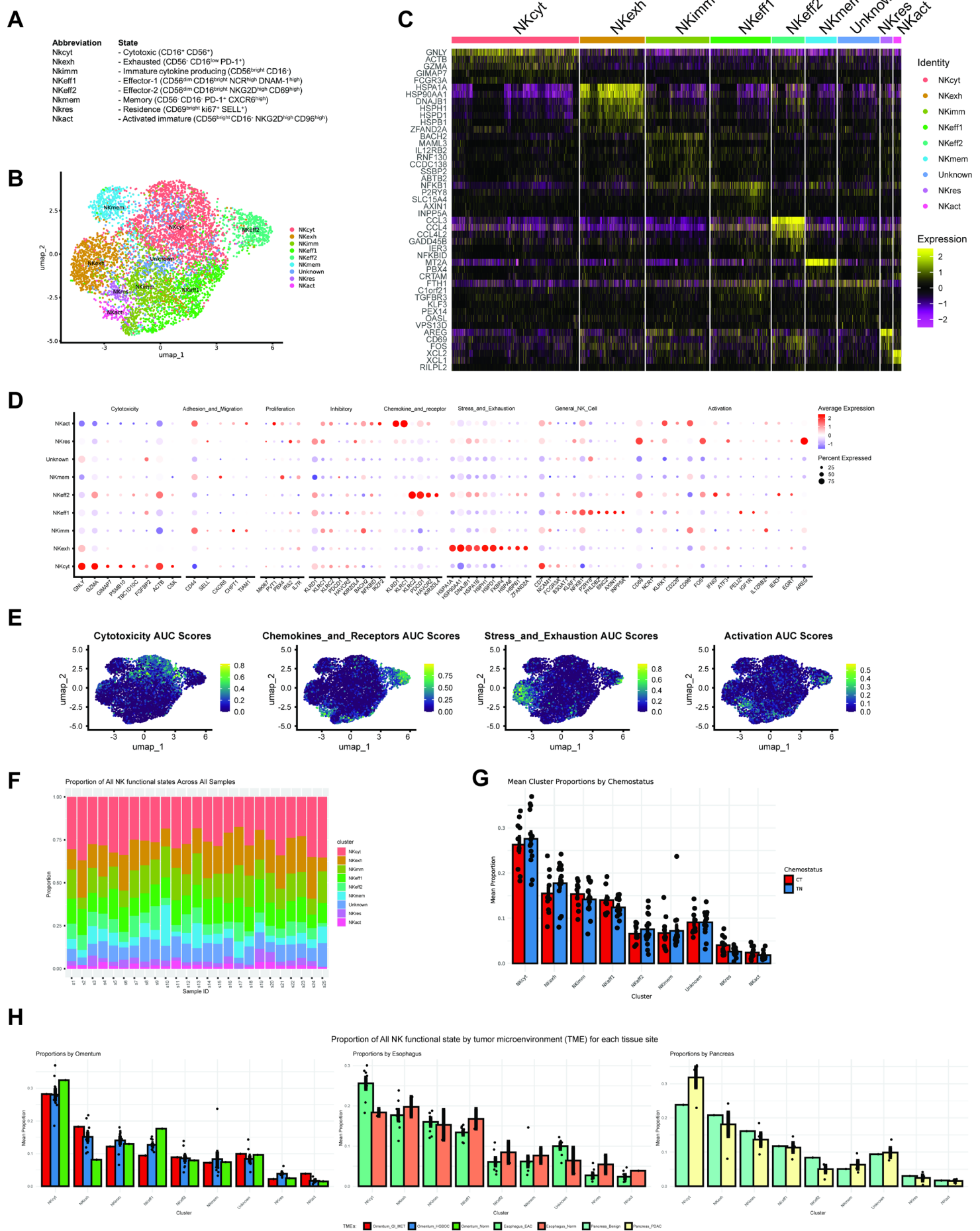


Figure 3: Major Lineage Identification Through Unsupervised Clustering. **A**, Eight NK cell functional states identified through purification of NK and unsupervised clustering: Cytotoxic (NKcyt), Exhausted (NKexh), Immature-cytokine-producing (NKimm), Effector-1 (NKeff1), Effector-2 (NKeff2), Memory (NKmem), Residence (NKres), and Activated-immature (NKact). **B**, UMAP visualization showing distinct clusters representing different NK functional states. **C**, Heatmap of top 10 differentially expressed genes (DEGs) for each functional cluster highlighting the unique molecular profiles. **D**, Functional gene sets based on literature review used to further characterize functional states of the distinct NK clusters based on their biological activities. **E**, UMAP feature plot of AUCell scoring cytotoxicity gene set, identifying NK cells with specific gene set potential. The gene sets are listing from left to right: cytotoxicity, chemokine and receptor, stress and exhaustion, and activation. **F**, Proportions of NK functional states across all samples. Bar chart of mean NK cluster proportions defined by chemotherapy status (**G**), and tissue microenvironment (**H**).

Pathway enrichment analysis, leveraging 1-vs-all differential pathway AUCells activity scoring, elucidates cluster-specific pathways that delineate the transcriptional profiles of NK cells, underscored by both statistical support and active gene expression within each gene set/pathway (Fig. 4). Utilizing high variable genes (HVGs), the pathways identified for each cluster distinctively represent the molecular phenotypes of NK cells (Fig. 4A, Table. S2). Notably, the NKexh cluster is predominantly characterized by the HSF1-dependent transactivation pathway (0.5 mean AUC), regulation of HSF1-mediated heat shock responses (>0.4 mean AUC), and attenuation phases (0.5 mean AUC), corroborating with data from Figure 3 that highlight these pathways as stress adaptation mechanisms⁵⁰, typical of exhausted NK cells within the tumor microenvironment⁵¹. These pathways are marked by the highest mean AUC values, indicating activity in up to 80% of the cells in this cluster. Although these stress-related pathways, particularly those involved in the heat shock response, they are notably less active in other clusters when compared to NKexh, as shown by individual cell activity in the NKexh cluster mapped on UMAP (Fig. 4B). Additionally, the NKeff2 cluster shows moderate activity for HSF-related pathways, displaying varied AUC levels within the cluster, which suggests an adaptive response to mitigate stress. This finding aligns with the interpretations from gene set activity analyses presented in Figure 3E. The NKeff1 cluster is another cluster of interest, showing involvement in the Erythropoietin-activated STAT5 pathway (0.3 mean AUC), known for enhancing tumor immunity by promoting NK cell viability⁵², although less than 50% of the cluster's cells exhibit activity in this pathway. Metal ion response pathways and EGFR-related pathways, each marked by a 0.25 mean AUC, are subtly active in the memory NK and resident NK clusters, respectively. These pathways, intimately linked with the tumor microenvironment, play critical roles in mediating TME interactions⁵³.

From a regulatory element perspective, encompassing regulons and transcription factors (TFs), the analysis (Fig. 4C, Table. S2) offers a deeper understanding of transcriptional alterations at the regulatory level, complementing the findings from the pathway analysis. It is important to note that the assessment of activity based on mean AUC values reveals lower activity due to the prevalence of TFs in the expression matrix of single-cell transcriptomics, highlighting the need for relative comparisons in regulon enrichment analyses. TF-enriched gene sets are associated with cellular metabolism and stress response, as illustrated by the targeting of DNA repair *ATM* genes⁵⁴ and the post-transcriptional regulator RBM17, which is part of the spliceosome machinery⁵⁵. Notably, the regulatory gene set targeting *HSF2* genes is up-regulated in the NKexh cluster relative to others, aligning with the highly active HSF-related pathways identified in the pathway enrichment analysis⁵⁶. Furthermore, a set of *PPARGC1A* (PGC-1 α) target genes is upregulated in the NKexh cluster, with 80% of the population showing activity. PGC-1 α , a key regulator of cellular metabolism and mitochondrial biogenesis, is essential for NK cells to adapt to metabolic stress conditions such as those found in TMEs and inflammation. It directly regulates the necessary cellular energy to sustain cytotoxicity and cytokine production capabilities⁵⁷. PGC-1 α has been implicated in countering tumor-induced NK dysfunction in cultured NK cells and represents a potential target for immunotherapy aimed at restoring NK functionalities in TMEs and facilitating NK adaptation to the microenvironment⁵⁸. AUCells UMAP visualization indicates that TFs targeting PGC-1 α are overwhelmingly active in the NKexh cluster (Fig. 4D). However, significant activity is also observed within the NKeff2 cluster, reflecting persistent molecular characteristics of TaNK-like NKeff2 profiles. This suggests a potential mechanism for TME-induced immune suppression in TaNK cells, consistent with the outcomes of the pathway activity analysis and gene set activities from Figure 3E.

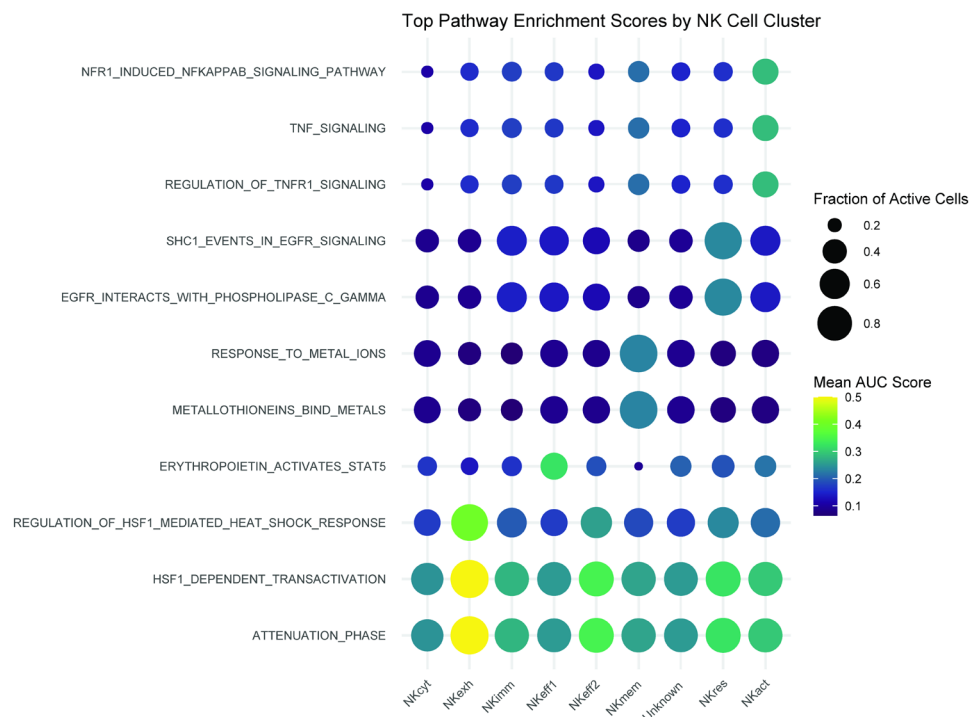
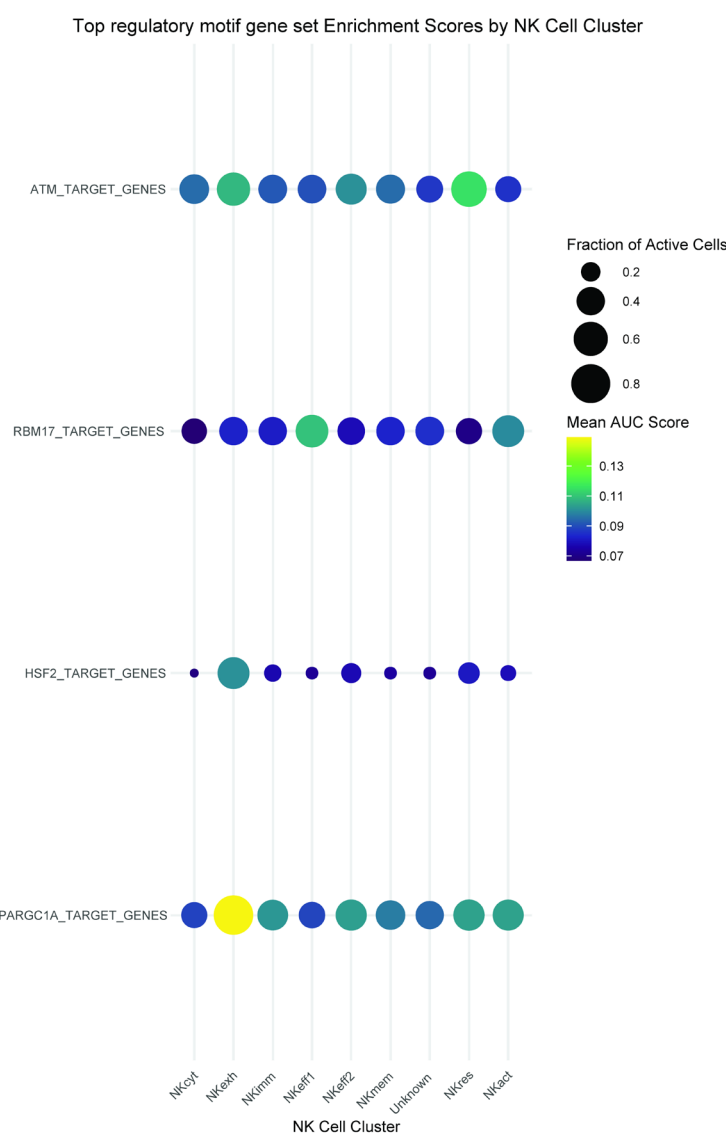
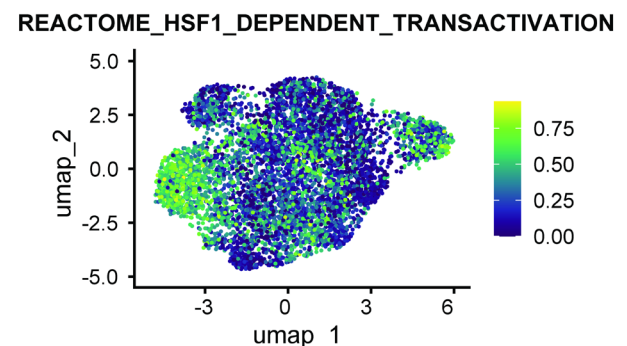
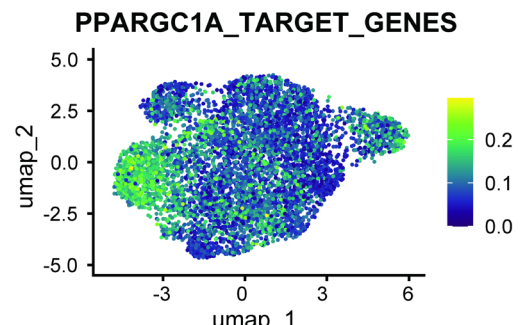
A**B****C****D**

Figure 4: Pathway Analyses Refine NK Functional Characterization. **A**, Dot plot visualizing the mean AUC values of top enriched pathway activity dominating each NK functional cluster, with dot size representing the percentage of active cells within each cluster population. **B**, Dot plot visualizing mean AUC values of top target genes of regulatory element motif among each NK functional cluster, with dot size indicating the active percentage within each cluster population. **C**, UMAP feature plot visualizing remarkable cellular stress-related pathways for heat shock factor-1 (HSF-1) dependent transactivation, emphasizing areas with heightened stress response (C), and regulatory motif targeting PPARGC1A gene set (PGC-1 α) (D). One-vs-all comparisons by Mann–Whitney U test, and Bonferroni correction for multiple comparisons. Criteria for detecting significant differences included a minimum of 25% average log-scale fold change and detectability in at least 25% of cells, a minimum of 2% average log-scale fold change, detectability in at least 25% of cells within either comparison group, a 1% significance level for a two-tailed test, and focusing only on positive differences (only.pos = TRUE). Cluster-specific filtering criteria included must exhibit more than 0.2 mean AUC values for at least one cluster, and less than 0.3 mean AUC values across all clusters (pathway), and demonstrate more than 0.1 mean AUC values for at least one cluster, and less than 0.2 mean AUC values across all clusters (regulon).

Effects of chemotherapy in mitigating tumor microenvironment-induced NK dysfunction.

The effects of chemotherapy appear to modulate NK cell transcriptomes, primarily focused on modifying stress responses, cellular adaptation, or enhancing NK cell-mediated tumor clearance. Activity heatmaps for gene set, pathway enrichment, and regulatory activities, based on chemotherapy status, are visualized through heatmaps of relative Z-score mean AUC (Fig. 5). Although chemotherapy does not uniformly affect NK gene set activity, it has reduced stress and exhaustion activities across all functional NK clusters, as evidenced by the decreased mean AUC of these gene sets, consistent across NK clusters (Fig. 5A, Table. S2). This highlights the impact of chemotherapy on NK phenotypes. The beneficial effects of chemotherapy on NK functionality are multifaceted; it may restore TME pressure on NK cells⁵⁹ or normalize the tissue microenvironment⁶⁰, leading to a downregulation of stress adaptation gene set activities. This is corroborated at the individual cell AUC level, where comparisons between chemotherapy-treated (CT, Fig. 5B top) and treatment-naïve (TN, Fig. 5B bottom) samples reveal variations in stress activities. Moreover, this chemotherapeutic influence on NK molecular profiles can negatively impact cellular proteostasis, as the stress adaptation gene set is involved in protein folding⁶¹. Additional analyses are necessary to distinguish the reduction in stress and exhaustion gene set activities from global direct cytotoxic effects on exposed cells, which present as all suppressive functionalities, including stress adaptation⁶², while simultaneously increasing activities in cell death-related pathways. Nevertheless, the cytotoxicity and general NK cellularity gene sets become more active post-chemotherapy in tumor-infiltrated NK clusters such as NKeff2 and NKexh, indicating favorable impacts of chemotherapy in restoring NK function from TME pressures.

For pathway enrichment activities, chemotherapy is observed to modulate HSF1-related pathways and attenuation phases, enhancing microenvironment interactions through FGFR2B receptor binding and activation (Fig. 5C, Table. S2)⁶³. NKeff1 and NKeff2 clusters show the most notable changes, particularly in the individual AUC scores of the HSF-1 transactivation pathway (Fig. 5D). The downregulation of heat shock protein pathways suggests a clearing of cellular adaptive states, reducing activities in heat shock response pathways post-chemotherapy, which supports the role of chemotherapy in improving microenvironment conditions. However, evidence of traditional chemotherapy effects that increase intracellular stress are also visible⁶⁴, reflected by heightened activities in EPO-related STAT5 activation across all clusters. Conversely, the broad decrease in activity in the activated NOXA mitochondrial translocation pathway, a component of the apoptosis cascade⁶⁵, suggests a stable cellular status in NK cells post-chemotherapy. Additionally, TNF signaling-related pathways' activities are suppressed in tumor-infiltrating NK clusters, while slightly more active in local tissue NK clusters such as NKmem and NKres, implying beneficial modifications of chemotherapy on NK functional restoration, while still contemplating the chemotherapeutic effects on microenvironment interactions and direct cytotoxicity. Alterations in EGFR-related and TGF-beta receptor signaling with increased activity after chemotherapy necessitate further investigations; these pathways are crucial for NK cell regulation, particularly in microenvironment interactions, and these complex molecular pathways could serve as potential targets for therapeutic development, given their involvement is extensively examined.

In the context of regulatory motif enrichment, following the trend observed in gene set and pathway activities, the activities of regulons targeting the HSF motif (*HSF4* and *HSF_Q6* motif) are suppressed across NK clusters post-chemotherapy (Fig. 5E, F, Table. S2). While the chemotherapeutic-induced down-regulation of HSF motif activity might suggest characteristics of exhaustion, the concurrent suppression of the PPARGC1A motif indicates potential adverse

effects on NK stability. PGC-1 α , critical for regulating NK cytotoxicity beyond its role in energy metabolism, hints at the NK cells' increased susceptibility to stress conditions. Furthermore, the regulon activity analysis reveals signs of chemotherapy-induced cellular stress: enhanced activities of DNA repair response (*ATM*) and reduced activities in nuclear stability (*NUP153*), transcription and translation machinery (*KAT5*, *SETD7*, *GTF2A2*), and cellular adhesion (*LAMB3*). These changes collectively diminish the viability of NK clusters. Conversely, *CARM1*, known to be vital in immune cell proliferation and differentiation⁶⁶, shows increased regulon activity post-chemotherapy in all clusters except NKexh, suggesting a distinctive alteration by chemotherapy in this specific cluster. These comprehensive analyses of NK gene sets, pathways, and regulatory motifs underscore the complex dynamics of chemotherapy on NK transcriptomes, highlighting potential adverse effects that weaken NK adaptive capabilities. However, they also suggest that chemotherapy can restore NK activation functions, illustrating its dual influence on NK cellular dynamics.

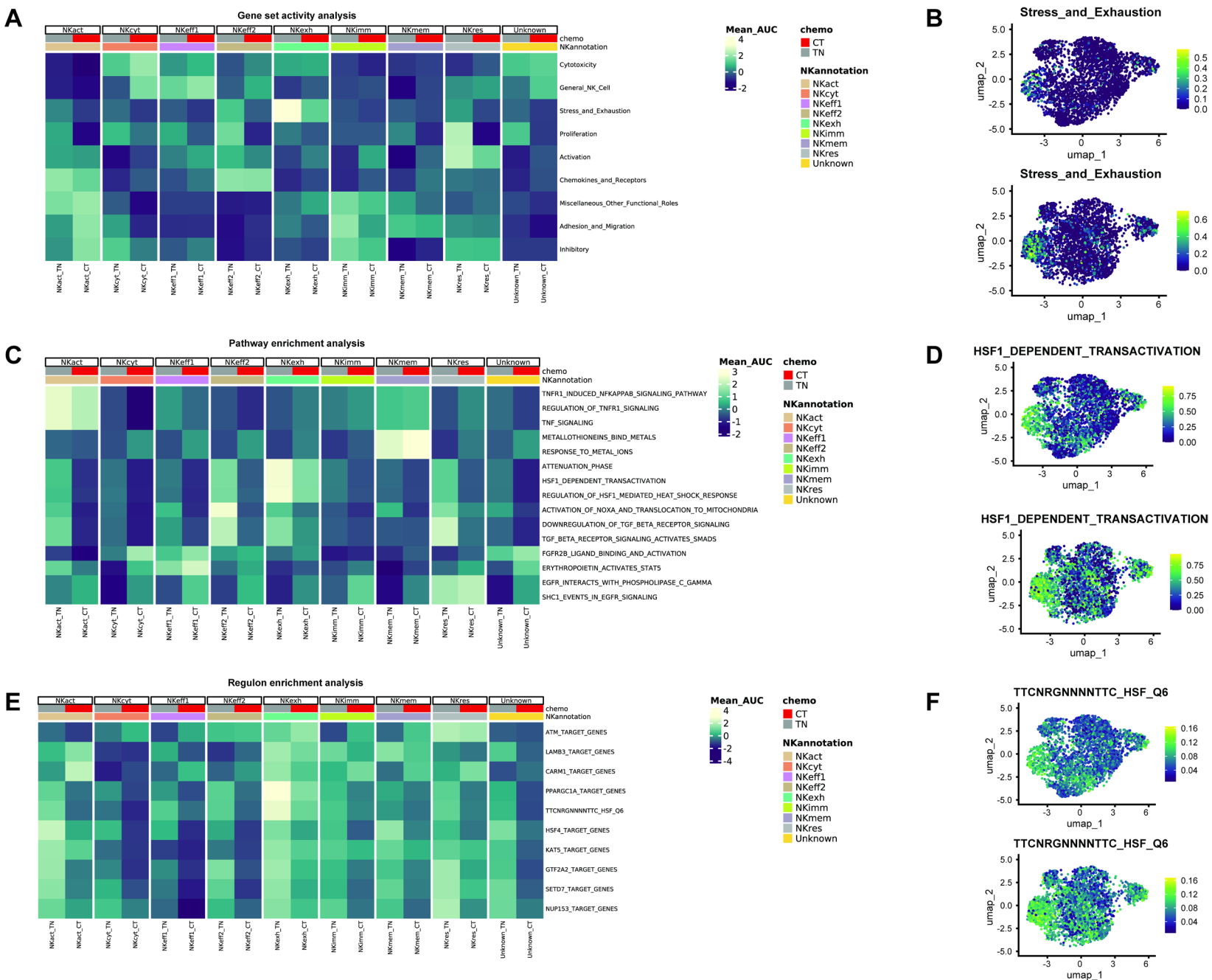


Figure 5: Chemotherapy impacts on transcriptional profiles of NK clusters. **A**, Heatmap showing the NK functional gene set activity based on chemotherapy status for each NK functional cluster, using relative Z-score mean AUC values. **B**, UMAP feature plot visualizing remarkable NK functional stress-related gene set, comparing between chemotherapy treated (top) and treatment naïve (bottom). **C**, Heatmap of top differentially active pathways, with relative Z-score mean AUC values illustrating chemotherapy status across NK functional profiles. **D**, UMAP feature plot visualizing AUC values of heat shock factor-1 (HSF-1) dependent transactivation (pathway), comparing between pre- (top) and post chemotherapy (bottom). **E**, Top differentially active transcription factor target gene sets heatmap manifesting implications of chemotherapy status via relative Z-score mean AUC values among NK molecular states. **F**, UMAP feature plot visualizing AUC values of highly conserved TTCNRGNNNNNTTC HSF Q6 motif, comparing between before (top) and after chemotherapy (bottom). One-vs-all comparisons by Mann–Whitney U test, and Bonferroni correction for multiple comparisons, with a 1% significance level for a two-tailed test.

Differential Impacts of Chemotherapy Responses Across Tissue-Specific NK Functional Clusters

It is crucial to assess the efficacy of chemotherapy across various tissues and tumor microenvironments (TMEs). Initial assessments focused on tissue microenvironment contributions (Fig. 6, Table. S2). Gene set activity analysis for each TME revealed microenvironment-specific activity statuses, despite general activity aligning with respective functional clusters on average (Fig. 6A). This is highlighted by the relatively high activity of stress and exhaustion in the NKexh cluster originating from pancreatic samples and adjacent normal esophageal samples, while adjacent normal from the omentum exhibited less activity in this gene set. Individual AUC comparisons emphasize this, showing functional NK cells from the pancreas (Fig. 6B top) in contrast to other samples (Fig. 6B bottom). PDAC samples displayed heightened proliferation activity across all NK clusters compared to other samples. Notably, NKcyt from adjacent normal and GI metastasis tumor tissues in the omentum showed high activity in cytotoxicity and general NK functions across several NK clusters, indicating a stratified underlying microenvironmental influence on defining NK molecular profiles.

In the pathway activity analysis, heatmaps illustrate cluster-specific enrichments based on tissue microenvironment (Fig. 6C, Table. S2). Three pathways are notably limited to specific tissues. For instance, Jun-c kinase signaling through TAK1 and P38/MAPK activation are predominantly active in NKeff2 and NKact clusters of esophageal adjacent normal samples, essential for NK activation and functionality^{67, 68}. Individual AUC analysis supports this, particularly noting active Jun-c kinase signaling in these samples compared to others (Fig. 6D). However, contributions from esophageal adjacent normal are subtle, despite being predominantly active in TAK1 Jun-c kinase signaling. Moreover, adjacent normal samples

from the omentum exhibit lower activity in HSF-1 heat shock response signaling across all NK clusters, consistent with gene set activity results.

For the regulatory section, activity scores are consistent across each tissue microenvironment and NK cluster (Fig. 6E, Table. S2). However, *LAMB3* gene regulation is particularly active in the NKmem of adjacent normal esophageal samples. Despite representing a small composition of the overall clusters, this regulatory activity is prominent in esophageal normal (Fig. 6F top) compared to other samples (Fig. 6F bottom). Adjacent normal omentum samples continue to exhibit persistent stress responses, such as *HSF4* regulation. The findings from tissue microenvironment analysis alone consistently indicate active NK cellularity, cellular adaptation, and functional activation in esophageal adjacent normals, while HSF-related signaling is broadly down-regulated in omentum counterparts. Chemotherapy status must be considered in interpreting these outcomes, as the adjacent normal omentum samples only contain chemotherapy-treated case, whereas both statuses are present in esophageal normal samples.

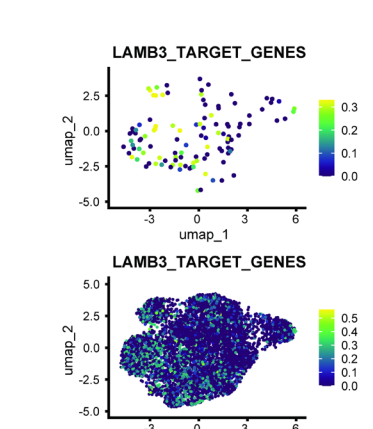
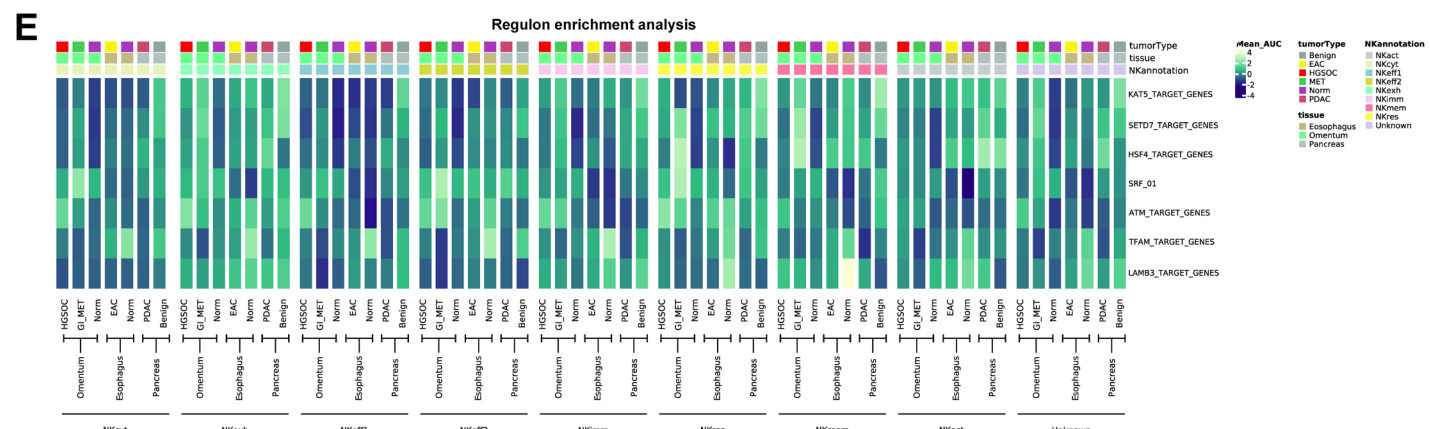
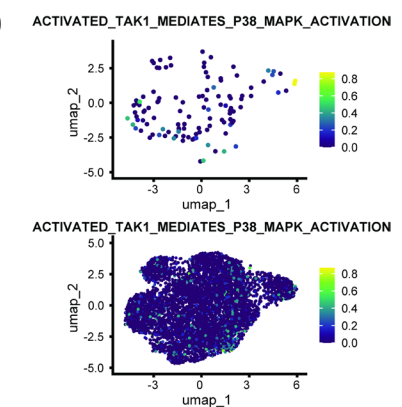
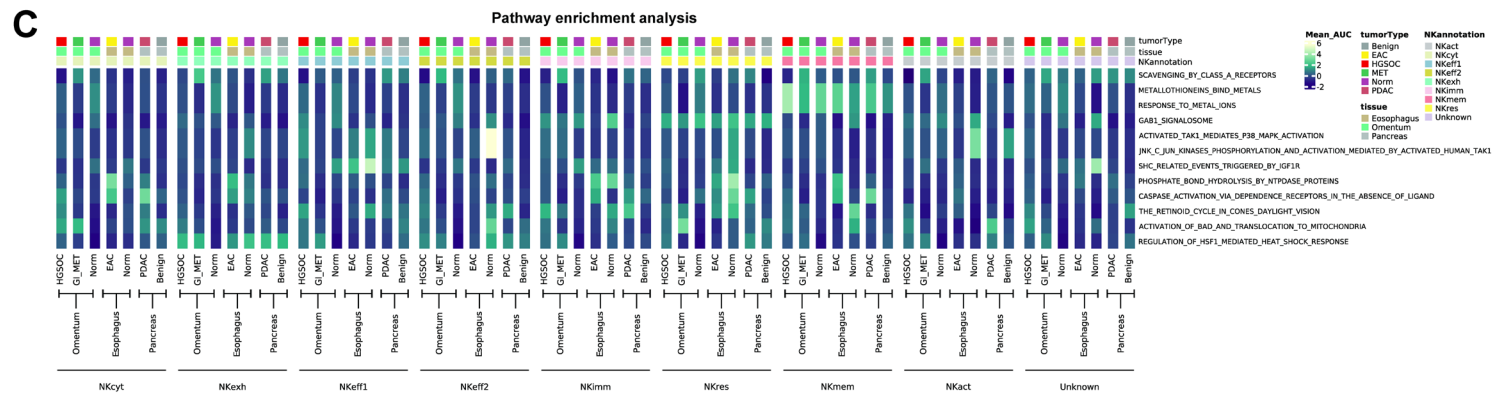
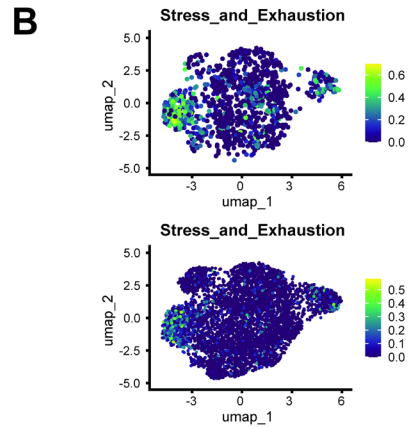
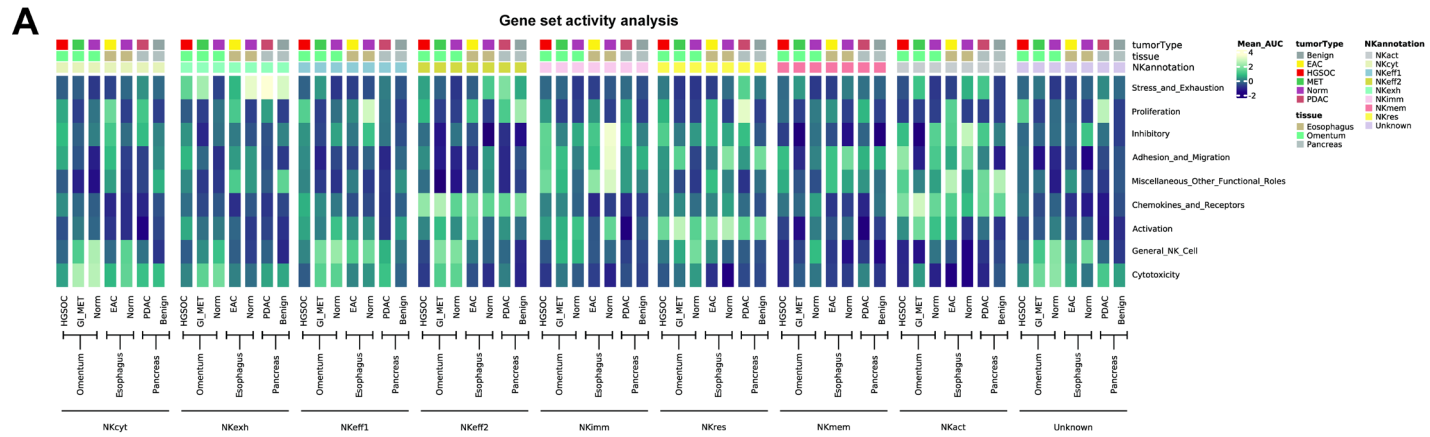


Figure 6: Tissue microenvironment-specific functional profiles of NK clusters. **A**, Heatmap showing the NK functional gene set activity based on tissue microenvironments for each NK functional cluster, using relative Z-score mean AUC values. **B**, UMAP feature plot visualizing remarkable NK functional stress-related gene set, comparing between pancreas tissue (top) and others (bottom). **C**, Heatmap of top differentially active pathways, with relative Z-score mean AUC values illustrating pathway activity of tissue microenvironment specific NK functional profiles. **D**, UMAP feature plot visualizing AUC values activated transforming growth factor beta activated protein kinase-1 (TAK1) mediates p38 mitogen-activated protein kinase (MAPK) activation (pathway), comparing between adjacent normal microenvironment (top) and others (bottom). **E**, Top differentially active transcription factor target gene sets heatmap manifesting implications of tissue microenvironment via relative Z-score mean AUC values among NK molecular states. **F**, UMAP feature plot visualizing AUC values of Laminin Subunit Beta 3 (LAMB3) target gene set, comparing between adjacent normal microenvironment (top) and others (bottom). One-vs-all comparisons by Mann–Whitney U test, and Bonferroni correction for multiple comparisons, with a 1% significance level for a two-tailed test.

As anticipated, the effects of chemotherapy vary among different TMEs (Fig. 7A). This variation is primarily attributed to the lack of resolution in assessing chemotherapy effects across NK clusters from the same functional state, indicating that chemotherapy efficacy is not uniformly applicable across specific TME conditions. The gene set activity outcomes reveal the actual impact of chemotherapy on prior results, with only minor improvements noted in reducing stress and exhaustion activity in NKexh across several sample groups, and becoming deleterious in esophageal adjacent normal post-chemotherapy. However, other NK clusters exhibited reduced stress activity, offset by other functions such as cytotoxicity and activation. Notably, cytotoxicity improved in adjacent normal esophageal samples post-chemotherapy for NKcyt and NKmem clusters. The lack of NKact in esophageal adjacent normal samples precludes conclusive comparisons. In contrast, comparisons between chemotherapy-treated and treatment-naïve adjacent normal esophageal samples suggest that chemotherapy benefits omentum normals by restoring NK functions, from reducing activity of stress and exhaustion to enhancing cytotoxicity and activation of NK cells. However, the absence of treatment naïve as comparative groups for omentum normal impedes activity comparisons between chemotherapy status.

Pathway enrichment results align with gene set findings (Fig. 7B), with the majority of chemotherapy effects on NK functional states showing minimal change between pre- and post-chemotherapy states within respective TMEs. While HSF-related pathway activities are suppressed in some NK clusters of adjacent esophageal tumors post-chemotherapy, all NK clusters in EAC, except NKcyt and NKact, show increased RUNX1 regulation targeting interleukin signaling in chemotherapy-treated versus treatment-naïve groups. This pathway is critical for enhancing both NK and NKT cell functions, such as cytotoxicity and interferon gamma production⁶⁹, particularly enhanced in EAC. The NKeff2 cluster shows the most notable improvement in this pathway following chemotherapy, suggesting initial functional

restoration in this TaNK-like cluster, which is heavily suppressed by TMEs. These results indicate potential benefits of chemotherapy in restoring NK functionalities in TMEs, despite remaining adverse effects. In contrast, chemotherapy effects on HGSOC are mostly deleterious, suggesting varied chemotherapy sensitivity based on tissue and TME conditions.

Regulon enrichment concurs with both gene set and pathway results (Fig. 7C). HGSOC remains susceptible to DNA damage, evidenced by heightened activity in ATM target regulation post-chemotherapy, and widespread suppression of NK adhesion and migration (LAMB3), and NK effector function (PPARGC1A, MAP2K1). However, moderate activity of CARM1 target regulation within adjacent normal omentum samples suggests chemotherapy benefits in restoring the exhausted state of NK clusters. For esophageal sample groups, chemotherapy appears beneficial, with indifferent or slight improvements in reducing ATM target gene set activity, alongside enhancements in NK functional signaling evident in gene set and pathway activity. The impacts of chemotherapy on NK transcriptomics consistently promote immune activation while presenting challenges for cell variability. The efficacy of chemotherapy is primarily determined by tissue microenvironment sensitivity, as documented from Figures 3 to 7, irrespective of the analysis grouping and observational resolutions.

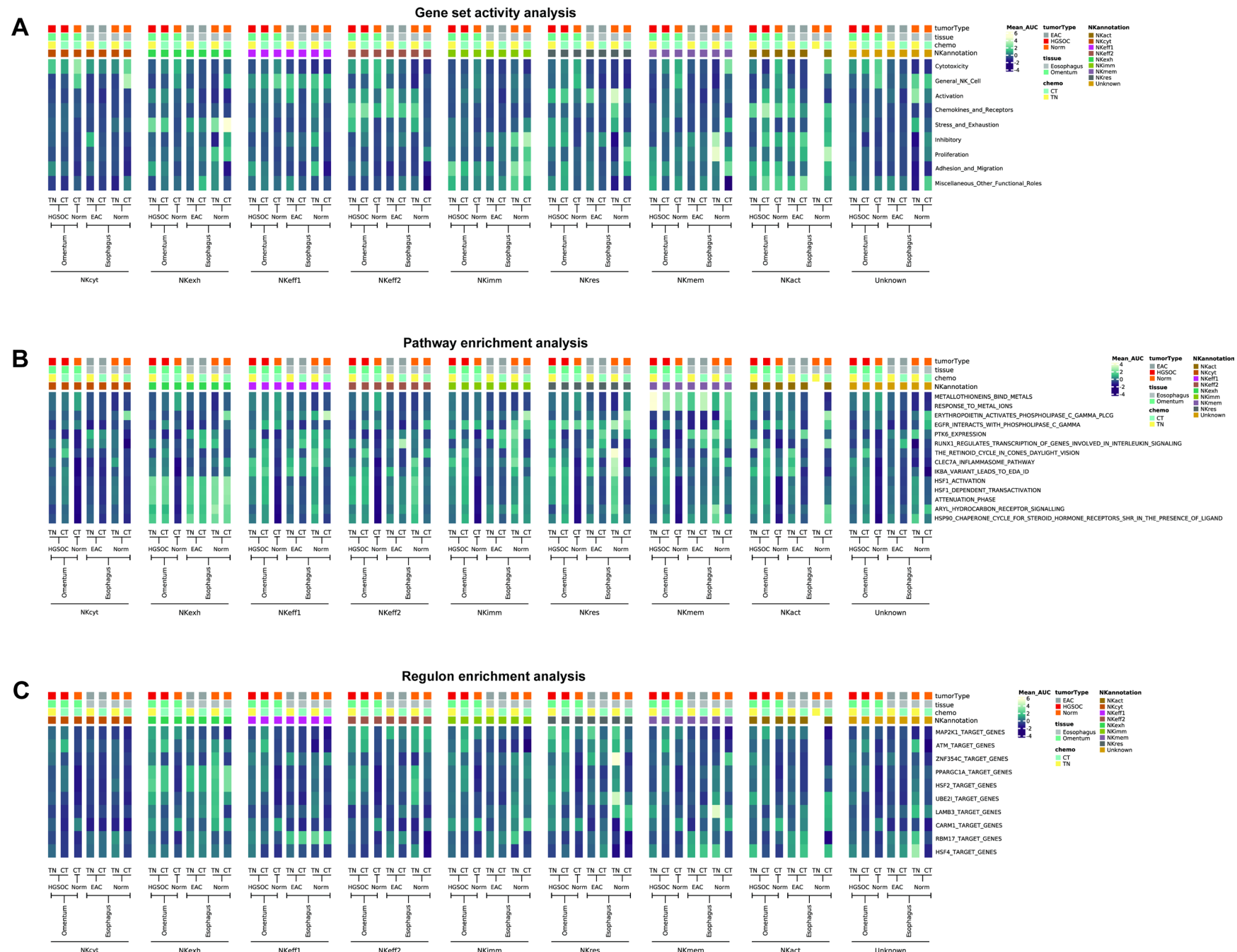


Figure 7: Tissue microenvironment-specific pathway/gene set activity profiles of NK clusters stratified by chemotherapy status. **A**, Heatmap showing the NK functional gene set activity based on tissue microenvironments for each NK functional cluster by chemotherapy status, using relative Z-score mean AUC values. **B**, Heatmap of top differentially active pathways, with relative Z-score mean AUC values illustrating pathway activity of tissue microenvironment specific NK functional profiles, defined by chemotherapy status. **C**, Top differentially active transcription factor target gene sets heatmap manifesting implications of tissue microenvironment based on chemotherapy status via relative Z-score mean AUC values among NK molecular states. One-vs-all comparisons by Mann–Whitney U test, and Bonferroni correction for multiple comparisons, with a 1% significance level for a two-tailed test.

Discussion

The NK functional profile has been systematically uncovered in this study, which utilized samples from three tissue sources to examine the transcriptional dynamics of tumor microenvironments (TME) under the influence of chemotherapy. The findings suggest potential fluidity in NK cell phenotypes and delineate the impacts of neoadjuvant chemotherapy on their transcriptional profiles.

While proportional analyses did not reveal statistically significant differences, the detailed characterization of various NK functional clusters proved to be insightful. Notably, clusters such as the exhausted NK and NK effector-2 exhibited clear signs of exhaustion and defective phenotypes⁷⁰. The NK effector-2 cluster, which closely resembles tumor-associated NK (TaNK) cells identified in recent pan-cancer studies based on *DNAJB⁺* expression profiles²³, was found to be influenced by TME factors that induce stress stimuli, reducing cytotoxic and effector capabilities.

Comprehensive functional characterizations using AUCells activity scores on NK functional gene sets, canonical pathway enrichment from Reactome, and regulatory motifs of transcription factors have consistently demonstrated a state of exhaustion within TMEs. This is particularly evident in the high activity of stress response pathways, notably those involving heat shock factor-1⁵⁰, alongside crucial transcription factors such as PGC-1 α ⁵⁸. These observations highlight that NK cell phenotypes are profoundly shaped by their microenvironments, underscoring the need for additional investigations.

Furthermore, molecular alterations highlighted by chemotherapy treatments reveal potential immunotherapeutic targets. The effects of chemotherapy in alleviating immune suppression are apparent, though they also bring about challenges in maintaining cellular

viability. The effectiveness of chemotherapy in restoring NK functionality appears to depend on the sensitivity of tissue microenvironment and transcriptomic states. From the data presented in Figures 3 through 7, it is suggested that utilizing beneficial chemotherapeutic effects on enhancing NK activation—such as through P38/MAPK and RUNX1 signaling pathways—while avoiding pathways that directly induce cytotoxicity or disrupt cellular homeostasis, like ATM signaling and PPARGC1A, could be viable strategies for targeted immunotherapy. However, given the molecular complexity and potential interactions among these pathways, further experimental validation through cell functional assays, such as cytotoxicity assessments of NK and NKT cells, is crucial to confirm the therapeutic implications of these molecular targets molecular profiling to aid cancer treatment strategies.

Several limitations warrant attention: computational approaches may not fully isolate NK clusters, and potentially excluding some cells, yet they help retain functional clusters from both NK and NKT cells. Purifying NK-NKT clusters from scRNA-seq data remains challenging, particularly due to T-cell contamination, a recurrent issue in NK single-cell studies. Further investigations are needed to assess potential purification biases or T-cell contamination. Moreover, all statistical analyses in this study were non-parametric, suitable for single-cell data yet constrained by the limited sample sizes of certain TME groups. Employing parametric statistical comparisons could provide more robust conclusions. Despite efforts to correct for batch effects, the heterogeneity of the data, especially from TMEs without defined chemotherapy statuses and the small sample size, might obscure subtle batch effects. Furthermore, factors such as age, gender, cancer duration, and family history were not considered in this study. Future research should investigate whether these factors influence NK functional states. Lastly, the adaptation of the AUCells-based differential pathway enrichment analysis from Python’s AnnData to R’s Seurat may affect its efficiency, necessitating further evaluation of this method in R. This study lays the groundwork for future explorations using

this approach, although the limited duration available for this dissertation might have constrained the breadth of characterizations possible. This focus on NK-cell characterization should be expanded in future studies to explore intermolecular interactions and cell-cell communications further.

Conclusion

Collectively, this study's findings elucidate the persistent NK cell dysfunction and heterogeneity across various tumor microenvironments, highlighting the consistent impact of chemotherapy on NK cell functionality. The tendencies indicated by activity scores reveal that specific changes occur within different TMEs, warranting further explorations. Moreover, the study supports the hypothesis that TMEs contribute to immune suppression in NK cells and sustain dysfunctional environments conducive to cancer progression. Observations of Chemotherapeutic impacts on NK functional states suggest that strategically enhancing NK cell activation, while minimizing cellular stress, could offer substantial benefits for targeted immunotherapies aimed at bolstering antitumor immune responses in cancer treatment.

Acknowledgement

The computational analyses conducted in this study were carried out on the University of Birmingham's BlueBEAR High-Performance Computing (HPC) service, which is provided to the university's research community. Further information about this service can be found at <http://www.birmingham.ac.uk/bear>.

Code availability

The R scripts used for data processing and analysis are available at https://github.com/ChisanuThumarat/MScBioinformatics_UoB_2324_Thesis_2588815.git.

Further details can be obtained from the thesis author or supervisors upon reasonable request.

Supplementary data availability

Supplementary data such as tables and figures are available at https://github.com/ChisanuThumarat/MScBioinformatics_UoB_2324_Thesis_2588815.git.

Further details can be obtained from the thesis author or supervisors upon reasonable request.

Appendix

Supplementary figure

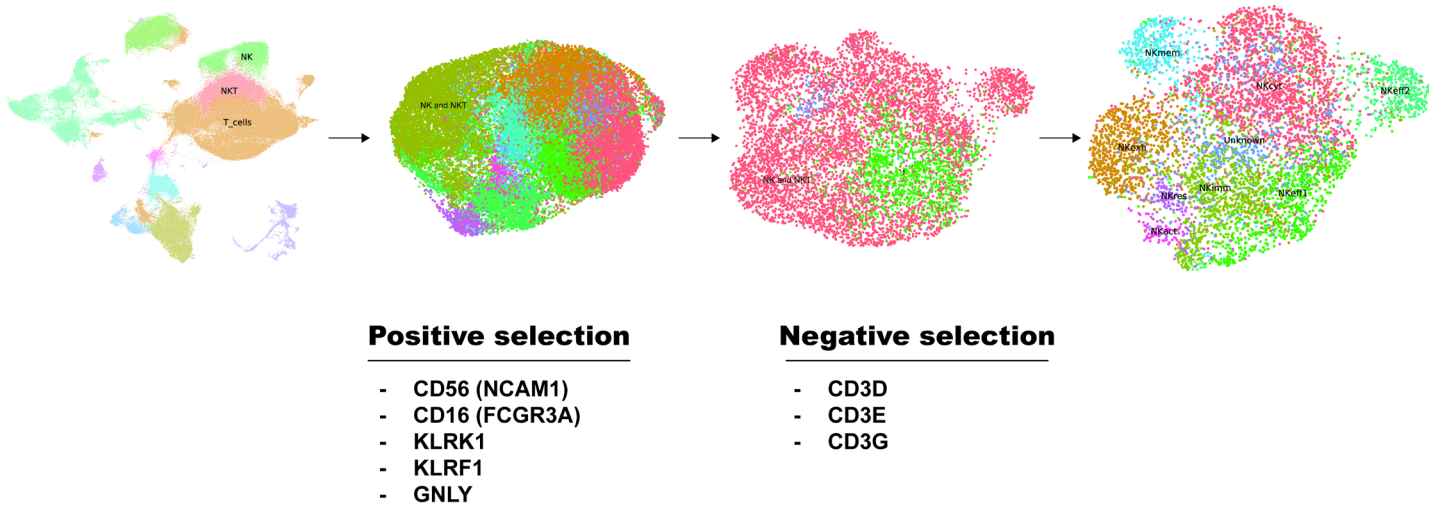


Figure S1: Unsupervised clustering analysis step to purify NK-NKT clusters. All unsupervised clustering analysis to NK-NKT isolation.

The NK-NKT clusters are selected based on positive and negative selection, presented in figure. With exception to the present of negative selection markers, if the positive selection markers are not completely having negative expression.

References

1. Chu J, et al. Natural killer cells: a promising immunotherapy for cancer. *Journal of Translational Medicine* **20**, 240 (2022).
2. Anfossi N, et al. Human NK cell education by inhibitory receptors for MHC class I. *Immunity* **25**, 331-342 (2006).
3. Cooley S, et al. A subpopulation of human peripheral blood NK cells that lacks inhibitory receptors for self-MHC is developmentally immature. *Blood* **110**, 578-586 (2007).
4. Pende D, et al. Killer Ig-Like Receptors (KIRs): Their Role in NK Cell Modulation and Developments Leading to Their Clinical Exploitation. *Frontiers in Immunology* **10**, (2019).
5. Vitale M, Cantoni C, Pietra G, Mingari MC, Moretta L. Effect of tumor cells and tumor microenvironment on NK-cell function. *European Journal of Immunology* **44**, 1582-1592 (2014).
6. Russ A, et al. Blocking "don't eat me" signal of CD47-SIRP α in hematological malignancies, an in-depth review. *Blood Rev* **32**, 480-489 (2018).
7. Paul S, Lal G. The Molecular Mechanism of Natural Killer Cells Function and Its Importance in Cancer Immunotherapy. *Frontiers in Immunology* **8**, (2017).

8. Jiang H, Jiang J. Balancing act: the complex role of NK cells in immune regulation. *Frontiers in Immunology* **14**, (2023).
9. Russick J, *et al.* Natural killer cells in the human lung tumor microenvironment display immune inhibitory functions. *Journal for ImmunoTherapy of Cancer* **8**, e001054 (2020).
10. Zhou Y, Cheng L, Liu L, Li X. NK cells are never alone: crosstalk and communication in tumour microenvironments. *Molecular Cancer* **22**, 34 (2023).
11. Pradeu T, Jaeger S, Vivier E. The speed of change: towards a discontinuity theory of immunity? *Nature Reviews Immunology* **13**, 764-769 (2013).
12. Liu CG, Chen J, Goh RMW, Liu YX, Wang L, Ma Z. The role of tumor-derived extracellular vesicles containing noncoding RNAs in mediating immune cell function and its implications from bench to bedside. *Pharmacol Res* **191**, 106756 (2023).
13. Zhang H, Ye L, Yu X, Jin K, Wu W. Neoadjuvant therapy alters the immune microenvironment in pancreatic cancer. *Frontiers in Immunology* **13**, (2022).
14. Okuda S, *et al.* Neoadjuvant chemotherapy enhances anti-tumor immune response of tumor microenvironment in human esophageal squamous cell carcinoma. *iScience* **26**, 106480 (2023).
15. Beckabir W, *et al.* Immune features are associated with response to neoadjuvant chemo-immunotherapy for muscle-invasive bladder cancer. *Nature Communications* **15**, 4448 (2024).

16. Galluzzi L, Humeau J, Buqué A, Zitvogel L, Kroemer G. Immunostimulation with chemotherapy in the era of immune checkpoint inhibitors. *Nature Reviews Clinical Oncology* **17**, 725-741 (2020).
17. Sadeghi S, Chen P-C, Jewett A, Kaur K. Chapter 14 - Combination of NK cell immunotherapy with chemotherapy and radiation enhances NK cell therapy and provides improved prognosis in cancer patients and in humanized BLT mouse model system. In: *NK Cells in Cancer Immunotherapy: Successes and Challenges* (eds Jewett A, Fong Y). Academic Press (2023).
18. Zingoni A, Fionda C, Borrelli C, Cippitelli M, Santoni A, Soriani A. Natural Killer Cell Response to Chemotherapy-Stressed Cancer Cells: Role in Tumor Immunosurveillance. *Front Immunol* **8**, 1194 (2017).
19. D'Alterio C, Scala S, Sozzi G, Roz L, Bertolini G. Paradoxical effects of chemotherapy on tumor relapse and metastasis promotion. *Seminars in Cancer Biology* **60**, 351-361 (2020).
20. Shuel SL. Targeted cancer therapies: Clinical pearls for primary care. *Can Fam Physician* **68**, 515-518 (2022).
21. Ouyang Y, et al. Combining single-cell and bulk RNA sequencing, NK cell marker genes reveal a prognostic and immune status in pancreatic ductal adenocarcinoma. *Scientific Reports* **14**, 15037 (2024).
22. Zhu Y, Wu X, Zhang Y, Gu J, Zhou R, Guo Z. Single cell transcriptomic analysis reveals tumor immune infiltration by NK cells gene signature in lung adenocarcinoma. *Heliyon* **10**, e33928 (2024).

23. Tang F, *et al.* A pan-cancer single-cell panorama of human natural killer cells. *Cell* **186**, 4235-4251.e4220 (2023).
24. Pazina T, *et al.* Alterations of NK Cell Phenotype in the Disease Course of Multiple Myeloma. *Cancers* **13**, 226 (2021).
25. Ziblat A, *et al.* Circulating and Tumor-Infiltrating NK Cells From Clear Cell Renal Cell Carcinoma Patients Exhibit a Predominantly Inhibitory Phenotype Characterized by Overexpression of CD85j, CD45, CD48 and PD-1. *Frontiers in Immunology* **12**, (2021).
26. Team RDC. R: A Language and Environment for Statistical.). R Foundation for Statistical Computing (2021).
27. Hao Y, *et al.* Dictionary learning for integrative, multimodal and scalable single-cell analysis. *Nat Biotechnol* **42**, 293-304 (2024).
28. McGinnis CS, Murrow LM, Gartner ZJ. DoubletFinder: Doublet Detection in Single-Cell RNA Sequencing Data Using Artificial Nearest Neighbors. *Cell Systems* **8**, 329-337.e324 (2019).
29. Hafemeister C, Satija R. Normalization and variance stabilization of single-cell RNA-seq data using regularized negative binomial regression. *Genome Biology* **20**, 296 (2019).
30. Choudhary S, Satija R. Comparison and evaluation of statistical error models for scRNA-seq. *Genome Biology* **23**, 27 (2022).

31. Korsunsky I, *et al.* Fast, sensitive and accurate integration of single-cell data with Harmony. *Nat Methods* **16**, 1289-1296 (2019).
32. Stelzer G, *et al.* The GeneCards Suite: From Gene Data Mining to Disease Genome Sequence Analyses. *Current Protocols in Bioinformatics* **54**, 1.30.31-31.30.33 (2016).
33. Park SY, Ter-Saakyan S, Faraci G, Lee HY. Immune cell identifier and classifier (ImmunIC) for single cell transcriptomic readouts. *Scientific Reports* **13**, 12093 (2023).
34. Guo C, *et al.* Single-cell transcriptomics reveal a unique memory-like NK cell subset that accumulates with ageing and correlates with disease severity in COVID-19. *Genome Medicine* **14**, 46 (2022).
35. Zhou L, Adrianto I, Wang J, Wu X, Datta I, Mi QS. Single-Cell RNA-Seq Analysis Uncovers Distinct Functional Human NKT Cell Sub-Populations in Peripheral Blood. *Front Cell Dev Biol* **8**, 384 (2020).
36. Liu X, *et al.* NK and NKT cells have distinct properties and functions in cancer. *Oncogene* **40**, 4521-4537 (2021).
37. Prager I, Watzl C. Mechanisms of natural killer cell-mediated cellular cytotoxicity. *Journal of Leukocyte Biology* **105**, 1319-1329 (2019).

38. Shimasaki N, Jain A, Campana D. NK cells for cancer immunotherapy. *Nature Reviews Drug Discovery* **19**, 200-218 (2020).
39. Korsunsky I, Nathan A, Millard N, Raychaudhuri S. Presto scales Wilcoxon and auROC analyses to millions of observations. *bioRxiv*, 653253 (2019).
40. Aibar S, *et al.* SCENIC: single-cell regulatory network inference and clustering. *Nat Methods* **14**, 1083-1086 (2017).
41. Zeng Z, *et al.* OmicVerse: a framework for bridging and deepening insights across bulk and single-cell sequencing. *Nature Communications* **15**, 5983 (2024).
42. Liberzon A, Birger C, Thorvaldsdóttir H, Ghandi M, Mesirov JP, Tamayo P. The Molecular Signatures Database (MSigDB) hallmark gene set collection. *Cell Syst* **1**, 417-425 (2015).
43. Wickham H. *ggplot2: Elegant Graphics for Data Analysis*. Springer International Publishing (2016).
44. Mangiola S, Papenfuss A. tidyHeatmap: an R package for modular heatmap production based on tidy principles. *Journal of Open Source Software* **5**, 2472 (2020).
45. Kassambara A. rstatix: Pipe-Friendly Framework for Basic Statistical Tests.) (2023).
46. Messaoudene M, *et al.* Mature Cytotoxic CD56bright/CD16+ Natural Killer Cells Can Infiltrate Lymph Nodes Adjacent to Metastatic Melanoma. *Cancer Research* **74**, 81-92 (2014).

47. Zhang QY, *et al.* Increased early activation of CD56dimCD16dim/- natural killer cells in immunological non-responders correlates with CD4+ T-cell recovery. *Chin Med J (Engl)* **133**, 2928-2939 (2020).
48. de Jonge K, *et al.* Circulating CD56bright NK cells inversely correlate with survival of melanoma patients. *Scientific Reports* **9**, 4487 (2019).
49. Casado JL, *et al.* Expansion of CD56(dim)CD16(neg) NK Cell Subset and Increased Inhibitory KIRs in Hospitalized COVID-19 Patients. *Viruses* **14**, (2021).
50. Xu Y, *et al.* Heat shock protein gp96 drives natural killer cell maturation and anti-tumor immunity by counteracting Trim28 to stabilize Eomes. *Nature Communications* **15**, 1106 (2024).
51. Tian W, *et al.* Chronic Stress: Impacts on Tumor Microenvironment and Implications for Anti-Cancer Treatments. *Frontiers in Cell and Developmental Biology* **9**, (2021).
52. Chanswangphuwana C, Allan DSJ, Chakraborty M, Reger RN, Childs RW. Augmentation of NK Cell Proliferation and Anti-tumor Immunity by Transgenic Expression of Receptors for EPO or TPO. *Mol Ther* **29**, 47-59 (2021).
53. Trotta R, *et al.* TGF- β Utilizes SMAD3 to Inhibit CD16-Mediated IFN- γ Production and Antibody-Dependent Cellular Cytotoxicity in Human NK Cells1. *The Journal of Immunology* **181**, 3784-3792 (2008).

54. Soriani A, *et al.* ATM-ATR-dependent up-regulation of DNAM-1 and NKG2D ligands on multiple myeloma cells by therapeutic agents results in enhanced NK-cell susceptibility and is associated with a senescent phenotype. *Blood* **113**, 3503-3511 (2009).
55. De Maio A, *et al.* RBM17 Interacts with U2SURP and CHERP to Regulate Expression and Splicing of RNA-Processing Proteins. *Cell Rep* **25**, 726-736.e727 (2018).
56. Fan Y, *et al.* Integrated Bioinformatics Analysis Identifies Heat Shock Factor 2 as a Prognostic Biomarker Associated With Immune Cell Infiltration in Hepatocellular Carcinoma. *Frontiers in Genetics* **12**, (2021).
57. Gerbec ZJ, *et al.* Conditional Deletion of PGC-1 α Results in Energetic and Functional Defects in NK Cells. *iScience* **23**, 101454 (2020).
58. Miranda D, *et al.* PGC-1 α -Dependent Mitochondrial Adaptation Is Necessary to Sustain IL-2-Induced Activities in Human NK Cells. *Mediators Inflamm* **2016**, 9605253 (2016).
59. Garofalo C, De Marco C, Cristiani CM. NK Cells in the Tumor Microenvironment as New Potential Players Mediating Chemotherapy Effects in Metastatic Melanoma. *Front Oncol* **11**, 754541 (2021).
60. Jain RK. Normalizing Tumor Microenvironment to Treat Cancer: Bench to Bedside to Biomarkers. *Journal of Clinical Oncology* **31**, 2205-2218 (2013).

61. Fan Y, *et al.* Integrated Bioinformatics Analysis Identifies Heat Shock Factor 2 as a Prognostic Biomarker Associated With Immune Cell Infiltration in Hepatocellular Carcinoma. *Front Genet* **12**, 668516 (2021).
62. Sharma A, Jasrotia S, Kumar A. Effects of Chemotherapy on the Immune System: Implications for Cancer Treatment and Patient Outcomes. *Naunyn Schmiedebergs Arch Pharmacol* **397**, 2551-2566 (2024).
63. Tsunematsu H, *et al.* Fibroblast growth factor-2 enhances NK sensitivity of hepatocellular carcinoma cells. *Int J Cancer* **130**, 356-364 (2012).
64. Mirzayans R, Andrais B, Murray D. Viability Assessment Following Anticancer Treatment Requires Single-Cell Visualization. *Cancers (Basel)* **10**, (2018).
65. Ploner C, Kofler R, Villunger A. Noxa: at the tip of the balance between life and death. *Oncogene* **27 Suppl 1**, S84-92 (2008).
66. Kumar S, *et al.* CARM1 Inhibition Enables Immunotherapy of Resistant Tumors by Dual Action on Tumor Cells and T Cells. *Cancer Discov* **11**, 2050-2071 (2021).
67. Huth TK, Staines D, Marshall-Gradisnik S. ERK1/2, MEK1/2 and p38 downstream signalling molecules impaired in CD56dimCD16+ and CD56brightCD16dim/- natural killer cells in Chronic Fatigue Syndrome/Myalgic Encephalomyelitis patients. *Journal of Translational Medicine* **14**, 97 (2016).

68. Li C, *et al.* JNK MAP kinase activation is required for MTOC and granule polarization in NKG2D-mediated NK cell cytotoxicity. *Proc Natl Acad Sci U S A* **105**, 3017-3022 (2008).
69. Seo W, Taniuchi I. The Roles of RUNX Family Proteins in Development of Immune Cells. *Mol Cells* **43**, 107-113 (2020).
70. Barshidi A, *et al.* The role of exhausted natural killer cells in the immunopathogenesis and treatment of leukemia. *Cell Communication and Signaling* **22**, 59 (2024).